Momentum dependence of 4*f* hybridization in heavy-fermion compounds: Angle-resolved photoemission study of $YbIr_2Si_2$ and $YbRh_2Si_2$

S. Danzenbächer,[1] Yu. Kucherenko,[1,2] D. V. Vyalikh,[1] M. Holder,[1] C. Laubschat,[1] A. N. Yaresko,[2,3] C. Krellner,[4] Z. Hossain,[4,5] C. Geibel,[4] X. J. Zhou,[6,7] W. L. Yang,[6,7] N. Mannella,[6,7] Z. Hussain,[7] Z.-X. Shen,[6] M. Shi,[8] L. Patthey,[8] and S. L. Molodtsov[1]

[1]*Institut für Festkörperphysik, Technische Universität Dresden, D-01062 Dresden, Germany*

[2]*Institute for Metal Physics, National Academy of Sciences of Ukraine, UA-03142 Kiev, Ukraine*

[3]*Max-Planck-Institut für Physik Komplexer Systeme, Nöthnitzer Strasse 38, D-01187 Dresden, Germany*

[4]*Max-Planck-Institut für Chemische Physik fester Stoffe, Nöthnitzer Strasse 40, D-01187 Dresden, Germany*

[5]*Department of Physics, Indian Institute of Technology, Kanpur-208016, India*

[6]*Department of Physics, Applied Physics and Stanford Synchrotron Radiation Laboratory, Stanford University, Stanford, California 94305, USA*

[7]*Advanced Light Source, Lawrence Berkeley National Laboratory, Berkeley, California 94720, USA*

[8]*Swiss Light Source, Paul Scherrer Institute, CH-5232 Villigen-PSI, Switzerland*

(Received 31 July 2006; published 8 January 2007)

Heavy-fermion compounds $YbIr_2Si_2$ and $YbRh_2Si_2$ were studied by means of angle-resolved photoemission (PE). The splittings and dispersions of the $4f^{13}$ bulk and surface PE signals in the region of the expected energy crossings of the 4*f* final states and the valence bands in the Brillouin zone are observed. The experimental results are explained in terms of a simplified periodic Anderson model by a momentum dependence of the electron hopping matrix element between the 4*f* and valence-band states.

DOI: 10.1103/PhysRevB.75.045109 PACS number(s): 71.27.+a, 71.20.Eh, 75.30.Mb, 79.60.−i

I. INTRODUCTION

In a series of rare-earth (RE) compounds, many-body interactions of the valence states with the strongly localized 4*f* states lead to heavy-fermion (HF) phenomena characterized by quasiparticle electronic bands of large effective masses.[1–4] On the other hand, due to their localized moments the 4*f* states are also mainly responsible for the magnetic properties of these systems. Of particular interest are scenarios where magnetic ordering via conduction-electron polarization (RKKY interaction[5]) is balanced by Kondo screening of the magnetic moments. Magnetic instabilities occur in the neighborhood of these so-called quantum critical points (QCP), and strong deviations from Fermi-liquid behavior are expected for the respective systems.[6] Although most RE based HF systems are Ce compounds, i.e., the famous HF superconductor $CeCu_2Si_2$,[7,8] Yb compounds like $YbRh_2Si_2$ may reveal similar phenomena and have attracted, therefore, considerable interest in the last few years.[9] In these compounds, Yb is close to a trivalent $[Xe]4f^{13}(5d6s)^3$ configuration, and the 4*f* hole ($4h^1$) takes the role of the $4f^1$ state in respective Ce compounds. $YbRh_2Si_2$ has a Kondo temperature (T_K) of about 25 K and is located on the antiferromagnetic side of a QCP. Even small changes of chemical composition may affect the 4*f* hybridization and drive the system through the QCP to the nonmagnetic regime. This is, e.g., achieved by replacing the 4*d* element Rh by the isoelectronic 5*d* element Ir: The isostructural compound $YbIr_2Si_2$ reveals a slightly increased hybridization and no magnetic ordering below its $T_K \sim 40$ K.[10]

For a deeper understanding of the underlying mechanisms more insight into the interaction of the 4*f* states with the valence band (VB) is required. While transport, specific heat and magnetization measurements give rather indirect information about these mechanisms, a more direct data may be expected from photoemission (PE) experiments, where electron correlations are reflected by the appearance of different electron configurations and multiplet effects. Analyzing these effects by means of the single-impurity Anderson model (SIAM)[11,12] allows for determination of the mean occupancy and the Kondo temperature and most PE data of RE systems have been discussed within this model.[8,13–15]

Nevertheless the question as to whether it is sufficient to treat the *f* states as localized impurities or the crystal symmetry has to be considered like in the periodic Anderson model (PAM)[16,17] remains a subject of extensive debates until now. Unfortunately, a satisfactory solution of PAM that takes into account a realistic band structure of non-*f* derived states is still missing. Most direct experimental insight into this problem may be expected from photoemission measurements of single-crystalline samples.

High-resolution PE experiments on single-crystalline samples of HF systems like $YbAl_3$,[14,18,19] $YbCu_2Si_2$,[14,18,20] YbB_{12},[21–24] and $YbInCu_4$ (Refs. 15 and 25–30) were performed and analyzed applying the single-impurity Anderson model. Thereby, controversial conclusions were derived about the applicability of the SIAM to the description of position, shape, and temperature dependence of the Kondo resonance in these systems.

Strong energy splittings and dispersions of the order of 0.2 eV were recently reported for the $4f_{7/2}$ surface component of $YbIr_2Si_2$ around the $\bar{\Gamma}$ point of the surface Brillouin zone (BZ) that clearly disregards any interpretation in the light of the SIAM.[31] A quantitative description, however, was possible in the framework of the PAM in the limit of infinite on-site Coulomb repulsion energy, U_{ff}. Dispersions of the $4f_{7/2}$ bulk component located in the close vicinity of the Fermi energy (E_F) were found to be much weaker than those

of the surface component. Instead, energy splittings and strong intensity variations of the $4f_{7/2}$ bulk signal were observed at the $\bar{\Gamma}$ point that were also reproduced by the PAM.

Energy splittings and dispersion were reported for the $4f^0$ "ionization" peak of a Ce(111) monolayer grown on W(110) and could be explained quantitatively by means of the same approach to the PAM.[32] Momentum (**k**) dependent intensity variations of the $4f^1$ "hybridization" peak similar to those observed for $YbIr_2Si_2$ were also measured for some Ce systems.[33–40] For $CePd_3$(111), these variations could satisfactorily be described in the framework of the PAM.[40] Dispersion of the Fermi-energy hybridization peak, however, if present at all, was found to be not larger than 30 meV.[33–38] The lack of dispersion may be related to the fact that for Ce systems only the occupied tail of the Kondo resonance can be sampled with photoemission. On the other hand, shape and intensity of the Fermi-level peak may heavily be influenced by dispersive states just above E_F (Ref. 8) making an interpretation in terms of a **k** dependence of the hybridization questionable.

In this contribution we present results of an angle-resolved PE study of the two closely related isostructural heavy-fermion compounds YbT_2Si_2 (T=Rh,Ir). In both cases, strong energy splittings and dispersions of the $4f$ signals and intensity variations of the $4f_{7/2}$ bulk emission are observed close to the expected intersection points of the $4f$ final states with the valence bands in the Brillouin zone. The observed **k** dependencies of the experimental data rule out unambiguously any interpretation in terms of the single impurity Anderson model. Instead, we show that they can correctly be described within a simple approach to the periodic Anderson model that takes into account a realistic description of the valence states, as provided by band-structure calculations.

II. EXPERIMENTAL DETAILS

A. Samples

The YbT_2Si_2 compounds studied here crystallize in the body-centered tetragonal $ThCr_2Si_2$- (I-) type structure[41] shown in Fig. 1. It reveals stacks of alternating elemental layers consisting of only one type of atoms (-T-Si-Yb-Si-T-). This kind of layered structure often allows to prepare clean surfaces as necessary for photoemission experiments by cleaving the samples in ultrahigh vacuum conditions. Note that the bonding to Si atoms is generally stronger for transition metals with chemically active nonfilled d shells of valence electrons than for ytterbium with the more inert $[Xe]4f^{14}6s^2$ atomic configuration. Therefore, the YbT_2Si_2 samples are easier to cleave between the Si and Yb layers. Since, however, the Yb atomic plane is neighbored on both sides with the identically arranged Si planes, the termination of the cleaved sample surface cannot be forecasted. As observed in our experiments, both Yb and Si surfaces as well as mixed terminations are statistically possible depending on slight variations of experimental conditions.

The samples were grown from In flux in closed Ta crucible and characterized by x-ray diffraction as well as by magnetic susceptibility, resistivity and specific heat measurements.[10] For $YbIr_2Si_2$ the obtained Kondo temperature $T_K \sim 40$ K is almost twice the value reported for $YbRh_2Si_2$.[9] Both compounds are close to a quantum critical point. In contrast to the Rh compound, no magnetic ordering below T_K was observed in the Ir compound. The resistivity behavior of YbT_2Si_2 is typical of heavy-fermion compounds with effective masses that are approximately 100 times larger than the free electron mass.

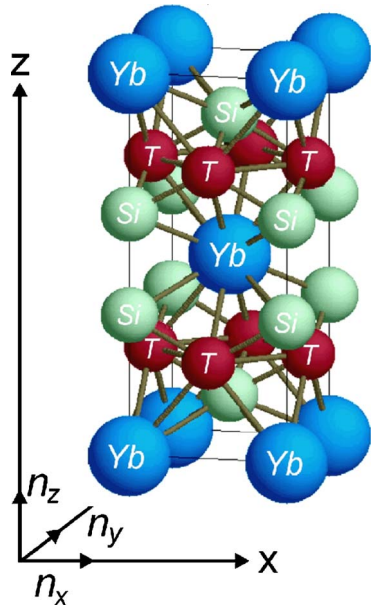

FIG. 1. (Color online) Crystal structure of YbT_2Si_2. Orthogonal unit vectors $\mathbf{n}_x$, $\mathbf{n}_y$, and $\mathbf{n}_z$ are set as described in the text.

B. Experimental conditions

Experiments on the $YbIr_2Si_2$ samples were carried out at the Advanced Light Source (ALS, beamline 10.0.1) exploiting experimental station HERS with a Scienta R4000 analyzer. During the experiments, the analyzer was rotated around the fixed $YbIr_2Si_2$ crystals in order to change collecting angle of electrons. The beam polarization was in the sample plane perpendicular to the $\bar{\Gamma}$-$\bar{M}$ direction in the surface Brillouin zone.

In order to describe the geometry of the ALS experiment, we introduce a coordinate system defining the orthogonal to each other unit vectors $\mathbf{n}_x$, $\mathbf{n}_y$, and $\mathbf{n}_z$. The latter is chosen to be parallel to the surface normal. The $\mathbf{n}_x$ and $\mathbf{n}_y$ vectors lie in the surface plane. The photon beam polarization was parallel to the $\mathbf{n}_y$ direction, with the beam in the (x,z) plane nearly at grazing incidence with the sample surface. The outgoing photoelectrons were detected in the (y,z) plane as well as in the planes derived from the (y,z) plane by its rotation around y axis.

The $YbRh_2Si_2$ samples were measured at the Swiss Light Source (SLS, Surface and Interface: Spectroscopy beamline) and the Berliner Elektronenspeicherring für Synchrotronstrahlung (BESSY, ID-03-1 BUS beamline) using a Scienta 2002 and a Scienta 100 spectrometers, respectively. Nearly

normal incidence radiation was applied. The analyzers were fixed, while the vertically positioned flakes of the $YbRh_2Si_2$ crystals were rotated. For linearly polarized radiation, the light-polarization geometry of the SLS experiment was similar to that used at ALS.

Each time 30°, 10°, and 8° photoemission cuts parallel to the $\bar{\Gamma}$-$\bar{M}$ high symmetry direction were covered at ALS, SLS, and BESSY, respectively. The YbT_2Si_2 single crystals were cleaved *in situ* by means of ceramic or metallic posts glued at the crystal surfaces in a vacuum better than 5×10^{-11} Torr. The samples were measured in the Kondo regime at a temperature of ~20 K. Angular and energy resolutions were set to 0.3° and 20 meV, respectively.

III. EXPERIMENTAL RESULTS

A. Angle-integrated photoemission

To determine the mean valence, the samples were first analyzed by means of angle-integrated PE. Spectra were taken at two different photon energies, $h\nu$=110 eV and 25 eV, in order to emphasize contributions of electronic states with different angular momentum character. At 110 eV photon energy the photoionization cross section of the RE 4*f* states is very high, while the ones of the Yb 5*d* and *T d* states are close to Cooper minima[42] and the intensity of the respective emissions is strongly reduced. The cross sections of *s* and *p* electrons are low as well at this photon energy. For $h\nu$=25 eV, the situation is reverse: The PE spectra are dominated by the signals of the valence states (mainly from *T d*).

These photon-energy dependent PE intensity variations for the $YbIr_2Si_2$ compound are demonstrated in the bottom in Fig. 2. The Ir 5*d*-derived bands measured at $h\nu$=25 eV are centered around 2.2 eV binding energy (BE) revealing a width of about 2 eV. At $h\nu$=110 eV, on the other hand, the contributions of the Yb 4*f* states are primarily monitored. Two $4f^{13}$ PE doublets appear close to E_F and at 0.9 eV reflecting signals from the bulk and the outermost surface layer, respectively, while a Yb $4f^{12}$ bulk final-state multiplet is observed between 5 and 13 eV BE.

Similar line shapes of the 4*f* emissions were measured for the $YbRh_2Si_2$ compound (Fig. 2, middle). In both cases, from the coexistence of the $4f^{12}$ and $4f^{13}$ bulk emissions a mixed-valent ground state could be concluded. The valence state of the YbT_2Si_2 compounds was derived from the intensity ratios of the bulk divalent and trivalent 4*f* configurations. To this end, the spectra were least-squares fitted by a superposition of the $4f^{12}$ and $4f^{13}$ multiplets.[43] Small deviations of the observed shape of the $4f^{12}$ multiplets from the calculated one can be ascribed to the experimental geometry, i.e., incidence angle and polarization of the light and were not considered. A weak integral background was used to account for nonelastic scattering contributions. Best fits were obtained with nearly symmetric Doniach-Sunjič line shapes convoluted by a Gaussian (Γ_G=20 meV) to account for the finite energy resolution of the experiment. Mean valence of ~2.9 was derived for the studied YbT_2Si_2 samples. Due to the above-mentioned uncertainties in the determination of the intensity of the $4f^{12}$ multiplet the error is relatively large (~0.05)

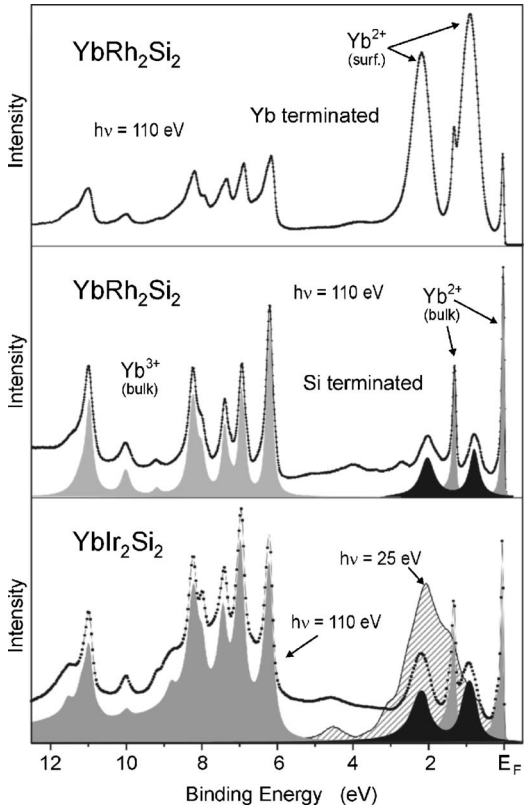

FIG. 2. Angle-integrated PE spectra of mainly Si terminated $YbIr_2Si_2$ taken at 25 eV (hatched) and 110 eV (dots) photon energy (bottom). Subspectra reflect results of a least-squares fit using atomic Yb $4f^{12}$ and $4f^{13}$ final-state multiplets (Ref. 43). Corresponding data of mainly Si (middle) and Yb (top) terminated $YbRh_2Si_2$.

smearing out possible differences in the valence of the Rh and Ir compounds expected from the different Kondo temperatures. The obtained valence close to the trivalent state of Yb is in accordance with the Kondo behavior reported for these compounds.[9,10]

Note that for both compounds, binding energy and intensity of the 4*f* surface signals vary from sample to sample reflecting the actual termination of the surfaces after each individual cleavage. In all experiments, however, the measured width of the 4*f* surface emission was rather small as compared to values usually observed for other Yb systems, indicating that the Yb atoms occupy predominantly equivalent surface sites in the YbT_2Si_2 samples under study. As shown in the two upper panels in Fig. 2, the surface contribution in the $YbRh_2Si_2$ sample can either dominate the whole spectrum (Yb topmost layer) or be almost negligible (Si termination). This fact causes certain difficulties in analysis of surface properties of YbT_2Si_2 crystals.

B. Angle-resolved photoemission

Figure 3 shows a series of angle-resolved PE spectra of $YbIr_2Si_2$ taken at a photon energy of 55 eV that allows observation of both Yb 4*f*- and VB-derived signals. The actual surface is predominantly terminated by a Yb layer as may be

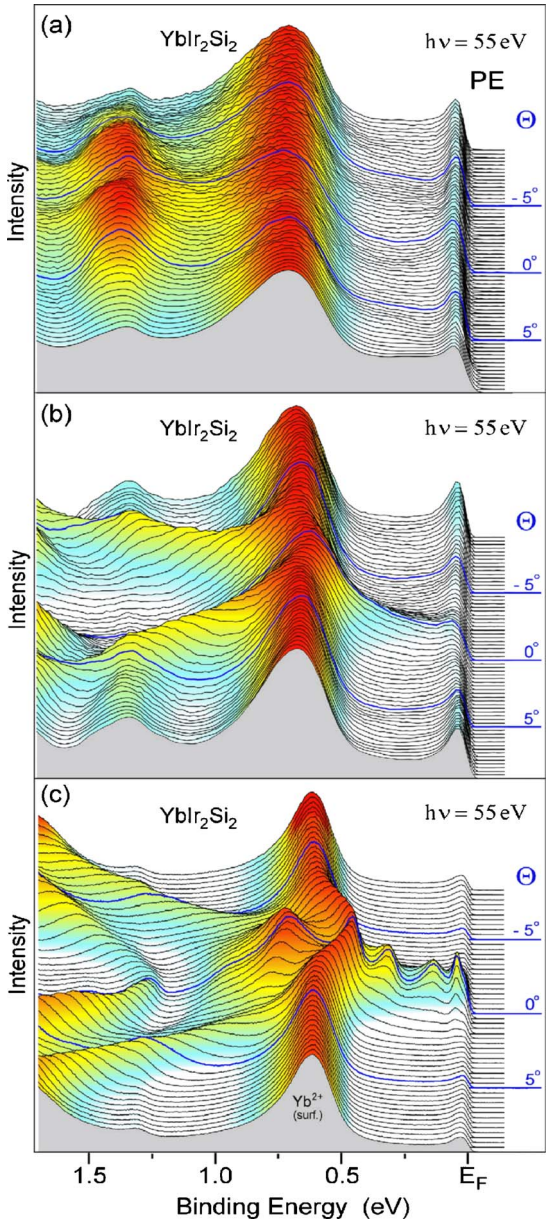

FIG. 3. (Color online) Angle-resolved PE spectra of $YbIr_2Si_2$ taken along the $\bar{\Gamma}$-$\bar{M}$ direction (bottom) and the two parallel to $\bar{\Gamma}$-$\bar{M}$ directions shifted (as shown in Fig. 9) by $\Delta\mathbf{k}_b$=0.19 Å^{-1} (middle) and $\Delta\mathbf{k}_a$=0.50 Å^{-1} (top) relative to $\bar{\Gamma}$-$\bar{M}$, respectively. Θ is polar detection angle. The spectra are normalized each to its maximum intensity.

concluded not only from the large intensity of the $4f_{7/2}$ surface signal but also from its low BE of 0.6 eV that indicates dense packing of the Yb atoms.[44] Angle-resolved PE spectra were measured along the $\bar{\Gamma}$-$\bar{M}$ direction [Fig. 3(c)] and the two parallel to $\bar{\Gamma}$-$\bar{M}$ directions in the surface BZ shifted by $\Delta\mathbf{k}_b$=0.19 Å^{-1} and $\Delta\mathbf{k}_a$=0.50 Å^{-1} relative to $\bar{\Gamma}$-$\bar{M}$, respectively [Figs. 3(b) and 3(a)]. The measurements along parallel to $\bar{\Gamma}$-$\bar{M}$ directions correspond to slices of the band structure by parallel planes (compare Fig. 9, top) and allow us to shift the VB-derived features relative to the $4f$ emission.

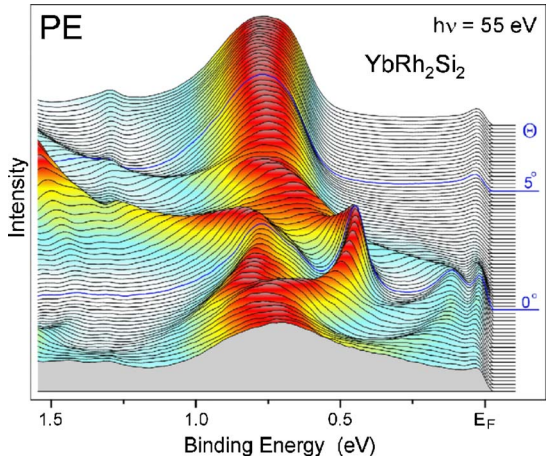

FIG. 4. (Color online) Angle-resolved PE spectra of $YbRh_2Si_2$ taken along the $\bar{\Gamma}$-$\bar{M}$ direction. The spectra are normalized each to its integral intensity. Note, that the surface-to-bulk ratio of the $4f$ signal is large indicating surface termination by an almost closed Yb layer (Ref. 44).

Two parabolic bands with holelike dispersion, from which one crosses the $4f_{7/2}$ surface emission around the $\bar{\Gamma}$ point in Fig. 3(c), are shifted in this way systematically away from E_F when going from the slice in the $\bar{\Gamma}$-$\bar{M}$ direction to the other slices [Figs. 3(b) and 3(a)]. Upon crossing with the parabolic band, the $4f$ surface signal reveals strong splittings and dispersions, that disappear if the intersection is lifted. Additionally, a strong anisotropy of the intensity close to E_F is observed in the region of the $\bar{\Gamma}$ point [Fig. 3(c)] combined with the appearance of at least two further spectral features between the $4f_{7/2}$ surface signal and the Fermi energy.

A very similar scenario is encountered for $YbRh_2Si_2$ (Fig. 4) with the only difference that the two parabolic bands are shifted toward E_F and the splittings of the $4f$ surface emission are obviously caused by interaction with the band at higher BE. The crossing of the band at lower BE that approaches the Fermi energy at the $\bar{\Gamma}$ point, affects the $4f$ signal much weaker.

The finding that dispersive properties of particularly $4f$ states are monitored can be proved by suppressing the VB emission at high photon energies. Figure 5 shows respective spectra of $YbRh_2Si_2$ taken at $h\nu$=110 eV where the $4f$ cross sections are much larger than those of the VB states and the spectra are, therefore, dominated by the $4f$ emission alone. Again, strong splittings and dispersions of the $4f_{7/2}$ surface signal are observed close to the $\bar{\Gamma}$ point, while the $4f_{5/2}$ component remains unaffected at this point in $\mathbf{k}$ space.

IV. BAND-STRUCTURE CALCULATIONS

In order to discuss the observed phenomena first the band structure of the systems was considered as may be described in the framework of the local density approximation (LDA). The bulk band structure of $YbIr_2Si_2$ and $YbRh_2Si_2$ are rather similar to each other as may be expected from the isoelectronic properties of the compounds.

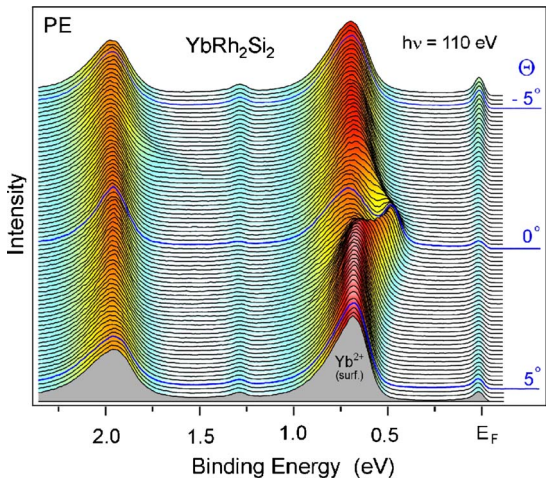

FIG. 5. (Color online) Angle-resolved PE spectra of $YbRh_2Si_2$ taken along the $\bar{\Gamma}$-$\bar{M}$ direction at $h\nu$=110 eV. The spectra are normalized each to its integral intensity.

To take into account surface effects, a nine-layer slab with (001) orientation of the surface was used. The surface atomic layer was formed by Yb atoms, then the Si, *T*, and again Si layers followed. The next Yb layer (the fifth atomic plane) was considered as a bulk layer. For this geometry, band-structure calculations were performed for both compounds by means of a fully relativistic version[45] of the linear-muffin-tin-orbital (LMTO) method.[46]

Figure 6 (left-hand side) shows results of band-structure calculations performed for $YbIr_2Si_2$. The 4*f* states appear as narrow spin-orbit-split bands close to E_F and at ~1.5 eV binding energy. For the surface layer almost the same BE position of the 4*f* bands is obtained as for the bulk. Due to hybridization effects the 4*f* state at the surface Yb atoms are still not filled: Even together with the contributions of *f* symmetry provided by the surrounding none-RE atoms the occupation of the $4f_{7/2}$ state in $YbIr_2Si_2$ is only 7.97. As a result, the surface $4f_{7/2}$ band is pinned at the Fermi energy, in contrast to the experimental observation. This clearly illustrates that LDA does not describe correctly the many-body properties of the *f* states.

In order to extract the valence-band structure of the $YbIr_2Si_2$ compound prior to hybridization with the 4*f* states, the calculations were also performed for a slab, where Yb atoms were replaced by divalent Ba in the outermost atomic layers and by trivalent La in the bulk (Fig. 6, right-hand side). Around Γ a group of mainly *T d*-derived parabolic bands with holelike dispersions is observed between 0.5 and 1.5 eV BE, region, where the surface contribution of the $4f_{7/2}$ states is expected. Another group of VBs with electronlike dispersions is found close to E_F crossing energy position of the bulk $4f_{7/2}$ states.

The results of the slab calculations for $YbRh_2Si_2$ are very similar to those obtained for the Ir compound, do not reveal, however, the experimentally observed shift of the bands toward the Fermi level. The band-structure calculations can reproduce the energy position of the valence bands if the number of valence electrons in the theoretical model is reduced. This can be done, e.g., if we force the mean Yb valency to be equal to 2.5 in the calculations. This value deviates, however, from the one estimated both from the spectroscopic and thermodynamic measurements (about 2.9), making this explanation unlikely. The number of valence electrons can also be reduced if the stoichiometry of the compound is slightly changed by removing part of the Yb atoms, i.e., assuming that in case of the $YbRh_2Si_2$ samples (Fig. 4) a large part of the surface was Si terminated. In fact, omission of the outermost Yb layer in the slab calculations leads to a shift of the bands by about 0.4 eV toward E_F that describes very well the situation encountered in the experiment.

The $YbRh_2Si_2$ PE data reflect then a superposition of contributions of both Si and Yb terminated parts of the surface, from which only the latter may be related to interaction with the 4*f* surface signal. This fact explains in a natural way why the interaction of the lowest BE parabolic band in Fig. 4 with the $4f_{7/2}$ surface component is negligibly weak, complicates the analysis, however, considerably. Surface-derived VB features may usually be discriminated from bulk emissions by their almost two-dimensional character reflected by lacking dispersion in the direction perpendicular to the surface. This method fails in the present case as can be seen in Fig. 7: The figure shows sets of PE spectra of an almost Si terminated $YbRh_2Si_2$ sample taken along the $\bar{\Gamma}$-$\bar{M}$ direction for different photon energies and, thus, different $\mathbf{k}_\perp$ values. In spite of this different $\mathbf{k}_\perp$ component, the parabolic bands do not shift in BE indicating almost two-dimensional character of all ob-

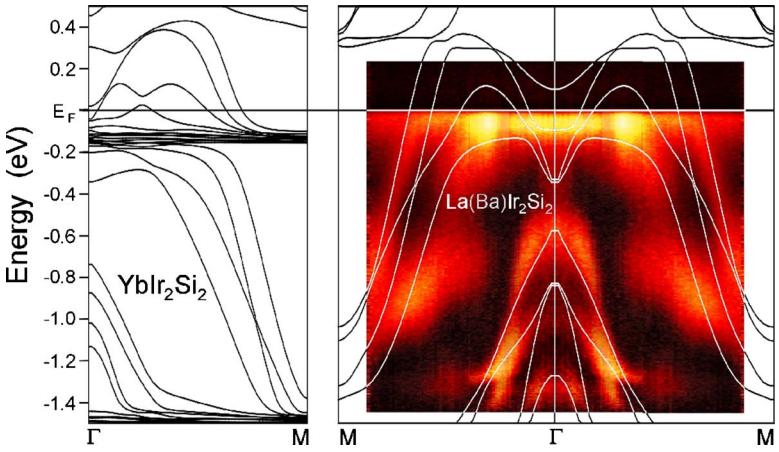

FIG. 6. (Color online) Band structure calculated along the Γ-*M* direction of the BZ for the nine-atomic layer $YbIr_2Si_2$ slab (left-hand side) and for the slab, where Yb atoms are substituted by Ba in the surface layer and by La in the bulk (right-hand side). Experimental data measured at $h\nu$=25 eV are shown in a color-scale representation. Lighter colors correspond to higher PE intensities.

served VB states. This behavior is, however, not necessarily an indication for surface-related states, but may be expected also for bulk states from the layered structure of the compound and the large lattice constant in the $\mathbf{n}_z$ direction, i.e., perpendicular to the surface. Due to the mentioned complications with the Rh compound we will focus in the following on the Ir compound and show, that the dispersive behavior of the $4f$ states may be explained on the basis of the calculated band structure by means of a simplified approach to the periodic Anderson model.

V. THEORETICAL MODEL

A. A simplified PAM

In order to describe the angle-resolved PE $4f$ data for YbT_2Si_2 compounds, we exploited a simplified periodic Anderson model that was recently successfully applied to explain the angle-resolved PE spectra of some Ce (Refs. 32 and 40) and Yb (Ref. 31) systems. Going beyond ground-state calculations (e.g., LDA+U approach[47]) our model allows to account for final-state interactions using only two experimentally derived parameters, namely, energy splitting and position of the $4f$ signals.

We consider the Anderson Hamiltonian,

$$H = \sum_{\mathbf{k},\sigma} \varepsilon(\mathbf{k}) d^+_{\mathbf{k}\sigma} d_{\mathbf{k}\sigma} + \sum_{\mathbf{k},\sigma} \varepsilon_f(\mathbf{k}) f^+_{\mathbf{k}\sigma} f_{\mathbf{k}\sigma} + \sum_{\mathbf{k},\sigma} V_{\mathbf{k}}(E) \times (d^+_{\mathbf{k}\sigma} f_{\mathbf{k}\sigma} + f^+_{\mathbf{k}\sigma} d_{\mathbf{k}\sigma}) + \frac{U_{ff}}{2} \sum_{i,\sigma} n^f_{i,\sigma} n^f_{i,-\sigma} = \sum_{\mathbf{k}} h_0(\mathbf{k}) + u, \tag{1}$$

where the VB states $|\mathbf{k}\sigma\rangle$ have a dispersion $\varepsilon(\mathbf{k})$ and are described by creation (annihilation) operators $d^+_{\mathbf{k}\sigma}$ ($d_{\mathbf{k}\sigma}$). The operator $f^+_{\mathbf{k}\sigma}$ creates an f electron with momentum $\mathbf{k}$, spin σ, and energy $\varepsilon_f(\mathbf{k})$. We assume that a nonhybridized f band has no dispersion, $\varepsilon_f(\mathbf{k}) = \varepsilon_f$. The two electron subsystems (VB and f states) are coupled via a hybridization $V_{\mathbf{k}}(E)$, where E denotes the BE with respect to E_F. Finally U_{ff} is the Coulomb repulsion between two f electrons localized on the same lattice site.

The main problem to treat the PAM is related to the term describing the local Coulomb interaction U_{ff}. The transformation of this term to a $\mathbf{k}$ representation leads to a mixing of states with different $\mathbf{k}$ values, which makes the problem difficult to handle quantitatively. For Ce systems neglecting weak contributions of $4f^2$ configurations to the initial and final states we decouple the valence states with different wave vectors $\mathbf{k}$. Then the Hamiltonian h_0 can be diagonalized for each particular $\mathbf{k}$ point of the surface Brillouin zone. This approximation corresponds to $U_{ff} \to \infty$ so that a double occupation of the f level is prohibited

For the $\mathbf{k}$-dependent hybridization matrix element $V_{\mathbf{k}}(E)$ we use the calculated respective f-projected local expansion coefficients $c_\nu(E,\mathbf{k})$ of the Bloch functions around the rare-earth sites (ν stands for the set of quantum numbers describing the local f contributions):

$$V_{\mathbf{k}}(E) = \Delta \cdot c_\nu(E,\mathbf{k}), \tag{2}$$

with Δ being a constant, adjustable parameter.

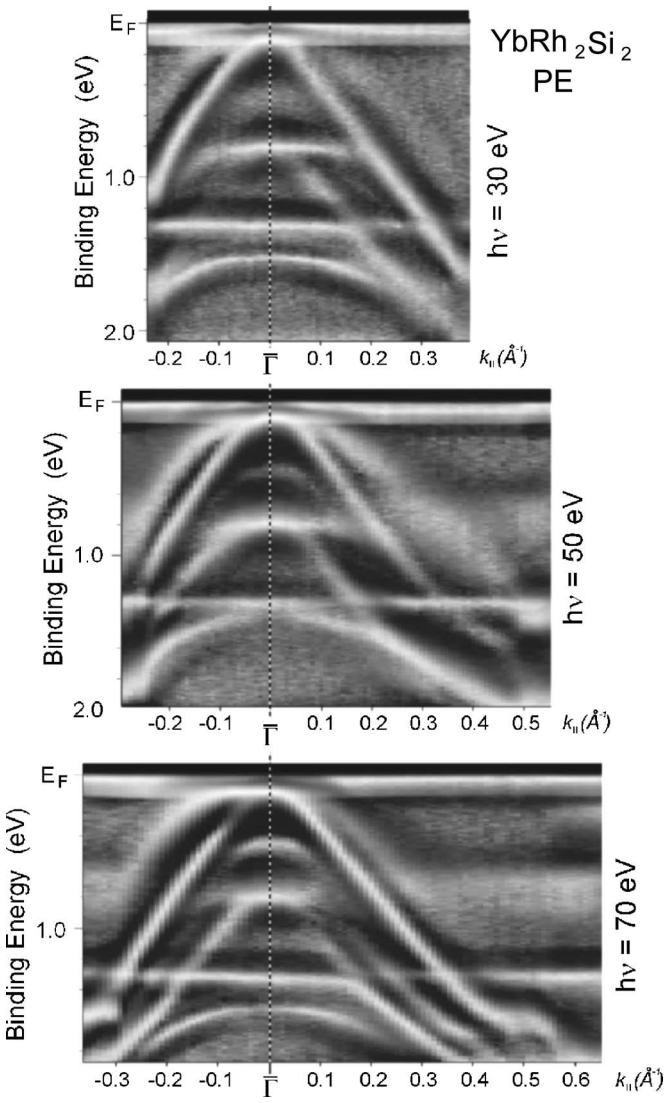

FIG. 7. Angle-resolved PE spectra of $YbRh_2Si_2$ taken along the $\bar{\Gamma}$-$\bar{M}$ direction at different photon energies. To emphasize band dispersions the spectra were normalized to equal intensities of all measured PE features. Lighter colors correspond to higher PE signals.

Diagonalizing the Hamiltonian matrix for the initial and final (electron-removal) states, we can calculate the spectral function for the $4f$ emission. This stage to solve the simplified PAM problem is formally similar to the one encountered in SIAM (as described in detail in Ref. 48) with the difference, however, that now the shape of PE spectra is changed as a function of $\mathbf{k}$.

Due to neglecting the $4f^2$ configurations in this model, only $4f^1 \to 4f^0$ transitions contribute to the PE intensity (I_f). In this case the experimental geometry can be taken into account in the spectral function

$$I_f(\mathbf{K}, E_{\mathrm{kin}}) = -\frac{1}{\pi} \mathrm{Im} \sum_n \sum_{\nu\sigma} \frac{|A^\sigma_\nu(\mathbf{K},\mathbf{e}) \langle f | f_{\mathbf{k}\sigma} | g \rangle|^2}{h\nu - E_{\mathrm{kin}} - (E^{(n)}_f - E_g) + i\tilde{\Gamma}}. \tag{3}$$

Here g is the ground state of the system with energy E_g and the sum should be calculated over all final states f (en-

ergy E_f) with one electron removed. E_{kin} is the photoelectron kinetic energy and $\tilde{\Gamma}$ represents the spectral broadening. The matrix element $\langle f|f_{\mathbf{k}\sigma}|g\rangle$ describes the transition of the many-electron system from the ground state g to the final state f by removing of an f electron. It defines mainly the energy distribution of the PE intensity because of all 4f-VB coupling effects involved here. The transition amplitude $A_\nu^\sigma(\mathbf{K},\mathbf{e})$ describes creation of a photoexcited electron with momentum $\mathbf{K}$ and spin σ by absorption of a photon with polarization $\mathbf{e}$. The momentum conservation requires $\mathbf{K}=\mathbf{k}+\mathbf{Q}$, where $\mathbf{Q}$ is a reciprocal lattice vector. This amplitude defines the intensity of the partial contribution ν of the initial 4f state and, consequently, one must sum over all these contributions.

In order to apply this approach to Yb compounds, we have to modify the formalism taking into account the nearly filled 4f shell of Yb. It seems more reasonable to consider f holes (h) instead of f electrons. After some algebra and redefining of model parameters, one gets as basis states the h^0 ($4f^{14}$), energy of which is set to zero, the h^1 ($4f^{13}$) corresponding to energy ε_f, and the h^2 ($4f^{12}$) configuration with energy $2\varepsilon_f+U_{ff}$, in analogy to the notation applied for electronic states in Ce compounds.[12,48]

In contrast to Ce, however, the h^2 configuration may be neglected only for the divalent surface atoms, while for the mixed-valent bulk atoms the h^2 term is essential for description of the $4f^{12}$ PE final state. Nonetheless, since the energy separation between the h^2 ($4f^{12}$) and the energetically nearly degenerated h^1 ($4f^{13}$) and h^0 ($4f^{14}$) configurations is large, h^2 admixtures to the ground state and, consequently, to the 4f configurations observed close to E_F are expected to be weak. Therefore, neglecting the h^2 admixtures may be allowed for a qualitative description of the $\mathbf{k}$ dependence of the 4f BEs in the energy region close to E_F.

B. Transition amplitude

Now we consider in detail the transition amplitude. It can be expressed as

$$A_\nu^\sigma(\mathbf{K},\mathbf{e}) = \sum_{lm} B_{lm}(\mathbf{K}) D_l \langle lm\sigma|\mathbf{e}\cdot\mathbf{n}|\nu\rangle, \tag{4}$$

where D_l is the complex radial matrix element, $B_{lm}(\mathbf{K})$ is the scattering path operator. If we neglect the scattering of the photoelectron wave at atoms surrounding the emitter,

$$B_{lm}(\mathbf{K}) = (-i)^l Y_{lm}(\mathbf{K}), \tag{5}$$

with a spherical harmonic Y_{lm} for the PE channel $|lm\sigma\rangle$. In this case, due to the dipole selection rules, for the PE from the 4f states we have only $l=2$ and $l=4$ for the angular momenta of outgoing photoelectrons (d and g waves). For a more general description of the PE including the experimental geometry we refer to Ref. 49.

Taking into account spin-orbit coupling, the functions used for the local expansion of the f bands are

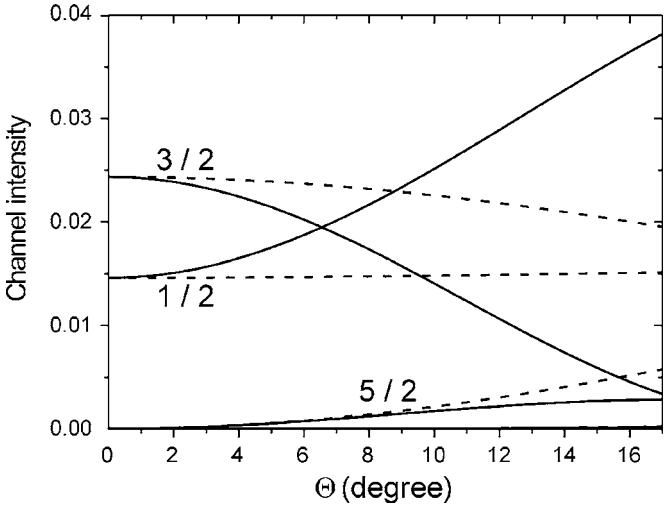

FIG. 8. Angular dependence of the $4f_{7/2}$ PE intensities in g (solid line) and d (dashed line) channels from different μ states for the experimental geometry used in the present work. Radial matrix elements D_l were set to 1 for the respective channel and to 0 for the other channel.

$$|\nu\rangle = |j\mu\rangle = \sum_\sigma C^{j,\mu}_{3,\mu-\sigma;(1/2),\sigma} Y_{3,\mu-\sigma}\chi_\sigma, \tag{6}$$

where μ is the z component of the momentum vector $\mathbf{j}$, $\sigma=\pm\frac{1}{2}$, and $C^{j,\mu}_{3,\mu-\sigma;(1/2),\sigma}$ are Clebsch-Gordan coefficients.[50]

In the case of the normal emission of the 4f electrons ($\mathbf{K}\|\mathbf{n}_z$) only terms with $m=0$ contribute to the transition amplitude. If the photon polarization is parallel to the emission direction ($\mathbf{e}\|\mathbf{K}$),

$$A^\sigma_{j\mu} = C^{j,\mu}_{3,\mu-\sigma;(1/2),\sigma}\frac{4D_4-3D_2}{\sqrt{28\pi}}, \tag{7}$$

with the condition $\mu=\sigma$. Thus, in this special case only 4f states having $\mu=\pm\frac{1}{2}$ are seen in the PE spectra. Considering the case $\mathbf{e}\perp\mathbf{K}$ ($\mathbf{e}\|\mathbf{n}_y$), we obtain for the transition amplitude the following expression:

$$A^\sigma_{j\mu} = C^{j,\mu}_{3,\mu-\sigma;(1/2),\sigma}\frac{i(D_4+D_2)\sqrt{3}}{\sqrt{28\pi}}, \tag{8}$$

with the condition $\mu=\sigma\pm1$, i.e., for this polarization direction of incoming photons the 4f states with $\mu=\pm\frac{1}{2}$ and $\mu=\pm\frac{3}{2}$ contribute to the PE spectrum. This case corresponds to experimental geometry for normal PE used for the experiments with $YbIr_2Si_2$.

For other PE directions the relative contributions of the μ states are changed. In Fig. 8 the PE intensities (squared transition amplitudes) are shown for g and d channels depending on the PE direction. For the g wave the $\mu=\pm\frac{1}{2}$ contributions (marked $\frac{1}{2}$ in the figure) increase considerably, whereas the $\mu=\pm\frac{3}{2}$ contributions strongly decrease with the increasing angle Θ. The $\mu=\pm\frac{5}{2}$ states contribute only weakly to the PE intensity, and the contribution from $\mu=\pm\frac{7}{2}$ states is negligible. The angular dependence for the d wave is not very strong. Taking into account the actual values of the complex

radial matrix elements (calculated absolute value of D_4 exceeds that of D_2 by factor 4) one can state that the g channel dominates in the total PE intensity over the d channel as well as over the channel-interference contributions. As a result, the angular dependence of the PE intensities from different μ states is close to the one calculated for the g channel.

The discussed angular dependence of the PE contributions for different μ explains variations of the spectral intensities in the angle-resolved PE spectra probing electronic states in the equivalent **k** points using different PE directions **K**.

VI. RESULTS AND DISCUSSION

First, model PAM calculations with a parabolic band located at different energies relative to a $4f$ state were performed (Fig. 9). To some extent this model reproduces a part of the electronic structure and experimental conditions relevant to measure angle-resolved PE spectra shown in Fig. 3. In Fig. 9 (top) the unhybridized f state is depicted by a plane at energy ε and the electronic band, that crosses the f state, is represented by a paraboloidlike $E(\mathbf{k})$ surface, as schematically depicted in the top panel in Fig. 9. Cutting this model band by the vertical planes **a**, **b**, and **c** leads to the respective two-dimensional representations shown in the insets in Figs. 9(a)–9(c) and simulates the experimental scenario depicted in Fig. 3.

The results of the model simulations are shown in panels (a), (b), and (c) in Fig. 9. If the energy gap between the $4f$ state and the top of the holelike band is rather large, the $4f$-VB interaction simply pushes the $4f$ state toward the Fermi energy. Since the interaction strength changes with the energy distance between the $4f$ and valence state, that is **k** dependent, a resulting narrow dispersion of the $4f$ state is obtained. One may expect that a similar mechanism can generally be applied to understand heavy-fermion phenomena in the region of the Fermi energy.

Crossing of $4f$ and VB states leads to a redistribution of the angular momentum character contributions into intensities of the two interacting states. The valence state gains more f character, while the initially pure f state picks up a character of the valence state. The discussed above two phenomena result in the **k**-dependent splitting of the f character state observed in the reported angle-resolved PE experiments.

For a more quantitative analysis of our $YbIr_2Si_2$ data, we used the VB structure of $La(Ba)Ir_2Si_2$ (Fig. 6, right-hand side) obtained by means of the LMTO slab calculations. This analysis represents an extension of work,[31] where the VB structure for PE simulation was approximated by three parabolic bands. Since due to symmetry requirements a coupling of the $4f$ states is only expected to the VB states with nonnegligible local f character at the Yb sites, we calculated the respective μ-projected local expansion coefficients $c_\mu(E,\mathbf{k})$ of the Bloch functions around the Yb sites. These values were then used in the hybridization matrix element $V_\mathbf{k}(E)$ (2) for the calculation of the μ contributions to the $4f$ spectral function. In order to improve the agreement with the experimental PE spectra the calculated energy bands were slightly constrained to the Fermi level. This transformation may be justified by the fact that in the calculations Yb atoms were substituted by Ba and La atoms with atomic radii different to the one of Yb.

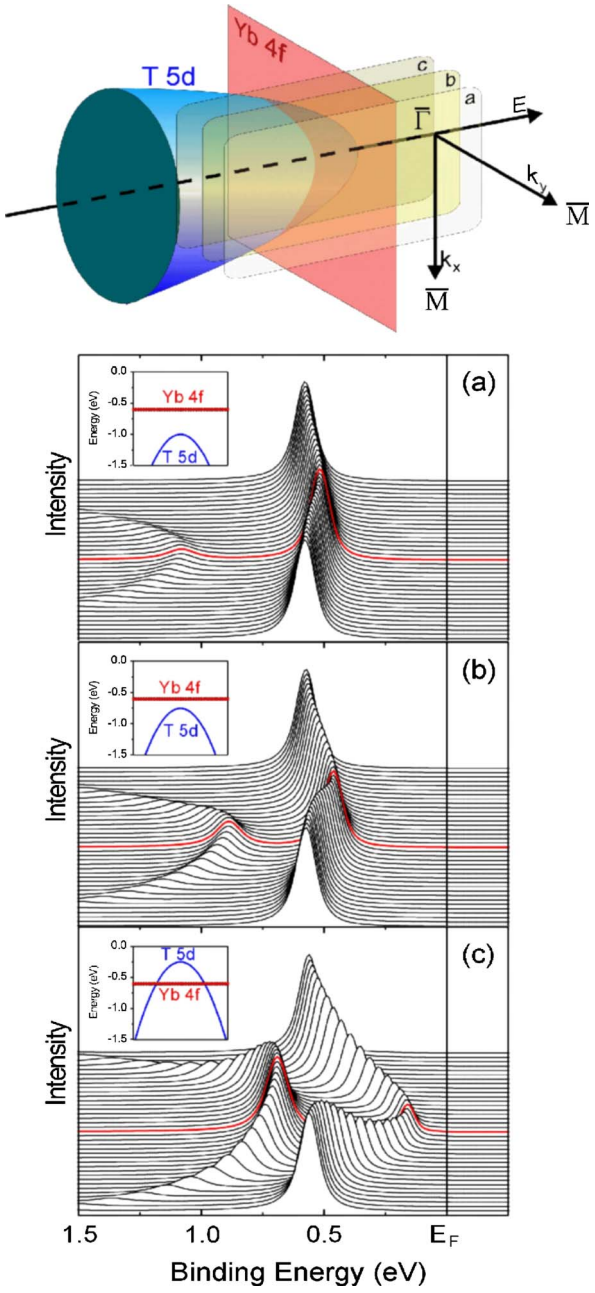

FIG. 9. (Color online) Results of the model PAM calculations performed for different slices of a paraboloidlike valence band. Calculated intensities show the f character of the hybrid bands describing qualitatively the scenarios observed in Fig. 3.

The next step was the calculation of the spectral function (3) on the basis of the simplified PAM assuming **k** conservation. Spectral functions were calculated independently for the individual layers of the slab and were finally superimposed by each other in order to simulate the PE spectra. To this end, contributions of the Yb surface layer and the next Yb layer were weighted by a factor of 0.71 and 0.29, respectively, in order to account for an exponential dependence of the escape depth of the $4f$ photoelectrons.

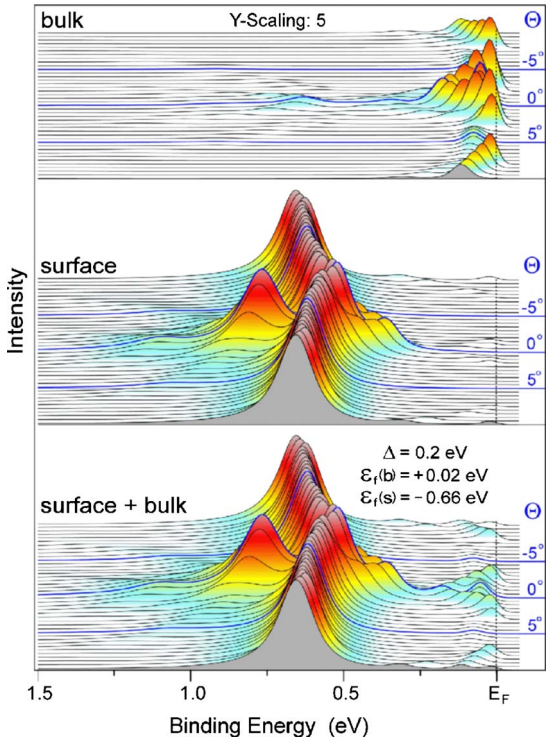

FIG. 10. (Color online) Angle-resolved 4*f* emission of $YbIr_2Si_2$ simulated by means of the simplified PAM: contribution from the bulk (top, multiplied by factor 5), the surface layer (middle) and the total intensity distribution in the PE spectra (bottom).

The numerical treatment is similar to that of the SIAM.[48] The fundamental difference, however, is that instead of a density of states integrated over the whole BZ a **k**-dependent energy distribution of VB states is used. A series of calculated spectral functions along the $\bar{\Gamma}$-$\bar{M}$ direction is shown in Fig. 10. The spectral functions were obtained using the parameters $\varepsilon_f(b)=0.02$ eV and $\Delta=0.2$ eV [for the surface, ε_f was lowered to $\varepsilon_f(s)=-0.66$ eV]. A choice of $\varepsilon_f(b)$ immediately above E_F was necessary, because the system is mixed valent with a mean valency close to 3. An estimate of $\varepsilon_f(s)$ is obtained from the observed BE of the unhybridized $4f_{7/2}$ surface signal and Δ is determined from the hybridization-induced maximum splitting of the 4*f* surface signal at the $\bar{\Gamma}$ point. The actual parameters were then derived from the best fit to the experimental data. Taking into account the recombination rate of the photoholes that increases with BE as reflected by the 4*f* linewidth, an energy dependent lifetime broadening of the form $\Gamma_L=0.01$ eV$+0.08E$ was used.[48] The calculated spectral functions were additionally broadened with a Gaussian ($\Gamma_G=20$ meV) to simulate the finite instrumental resolution.

Beginning with the discussion of the surface component, the calculated spectra shown in the middle in Fig. 10 reproduce nicely the observed dispersion of the 4*f* states around the $\bar{\Gamma}$ point. The large splitting of the main surface emission around 0.7 eV BE is due to the formation of symmetric and antisymmetric linear combinations of the 4*f* and VB orbitals lifting the energy degeneracy of these states. Since the energy splittings and the corresponding dispersions are restricted to certain regions in **k** space, they lead in angle-integrated spectra to a broadening of the surface signal attributed so far exclusively to coordination effects.[44] The feature at 0.35 eV appears due to the top of the parabolic VB with electronic states containing mainly μ components which cause negligible contributions to the transition amplitude. As a result, 4*f* hybridization effects observed at this VB are much weaker. In addition to the splitting of the main 4*f* surface component, further *f*-derived surface features appear at lower BE. These structures arise from *f* admixtures to valence bands laying at lower binding energies.

In the case of the bulk emission, no *f* contributions around E_F are expected without hybridization at $T=0$ K, because the divalent $4f^{14}$ configuration lies above the Fermi energy and is unoccupied. For finite hybridization and a VB state around 0.05 eV BE at the $\bar{\Gamma}$ point, however, two peaks appear in the simulated PE spectra at about 0.05 eV and 0.15 eV BE as observed in the normal emission experiment (Fig. 10, upper panel). These peaks reflect symmetric and antisymmetric linear combination of the $4f^{13}$ and $4f^{14}$ configurations. Deeper lying VB states cause additional features at correspondingly higher BEs, the intensities of which decrease with increasing binding energy. The lowest lying *f*-derived feature appears at the BE of the lowest occupied VB and reveals the same dispersion as the latter with the consequence that the feature disappears at the crossing of the Fermi energy by the VB state.

Superposition of the bulk and surface contributions in the bottom of Fig. 10 yields good agreement with the experimental data. One may notice, however, that even far from the $\bar{\Gamma}$ point finite spectral weight at E_F is observed in the experimental data that is not reproduced by our numerical approach. This feature may be assigned to thermal excitation into the bulk 4*f* state closely above E_F.[8] On the other hand, effects of finite U_{ff} and interaction of the 4*f* with unoccupied VB states, that were not considered in the present model, may also contribute to this peak.

VII. CONCLUSIONS

We have found that the 4*f* states in $YbIr_2Si_2$ and $YbRh_2Si_2$ are subject to strong **k**-dependent splittings and dispersions, a behavior, which cannot be understood in the framework of the single-impurity Anderson model. Instead, the 4*f* angle-resolved PE data could be correctly described within a simple approach to the periodic Anderson model in the limit $U_{ff}\rightarrow\infty$. In this approach, energy splittings and dispersions of the 4*f* states are predicted for those points in **k** space, where the VB states are degenerate in energy with the unhybridized $4f^{13}$ configurations. Since for mixed-valent systems this condition is particularly fulfilled at the Fermi surface, our results may have strong impact on the understanding of the HF properties and electron-correlation phenomena in the region of the quantum critical points in these systems.[51] The dispersive properties of the 4*f* states explain in a natural way the observed broadening and line shape anomalies in angle-integrated PE spectra of many Yb systems as well as discrepancies between the angle-resolved PE data of different authors.

ACKNOWLEDGMENTS

This work was funded by the Deutsche Forschungsgemeinschaft, SFB 463, projects TP B4, and TP B16, and the BMBF, project 05-SF8OD1/4. The experiments at the ALS were supported by the DOE Office of BES, Division of Material Science, with Contract No. DE-FG03-01ER45929-A001. The work at Stanford was also supported by NSF Grant No. DMR-0304981 and ONR Grant No. N00014-98-1-0195-P0007.

[1] P. Fulde, *Electron Correlations in Molecules and Solid* (Springer, Heidelberg, 1995).
[2] P. Wachter, in *Handbook on the Physics and Chemistry of Rare Earth*, edited by K. A. Gschneider, L. Eyring, G. H. Lander, and G. R. Choppin (Elsevier Science, Amsterdam, 1994), Vol. 19.
[3] L. Degiorgi, Rev. Mod. Phys. **71**, 687 (1999).
[4] A. C. Hewson, *The Kondo Problem to Heavy Fermions* (Cambridge University Press, Cambridge, 1993).
[5] L. B. Robinson, L. N. Ferguson, Jr., and F. Milstein, Phys. Rev. B **3**, 1025 (1971).
[6] J. A. Hertz, Phys. Rev. B **14**, 1165 (1976); A. J. Millis, *ibid.* **48**, 7183 (1993); M. A. Contenintino, Phys. Rep. **239**, 179 (1994).
[7] F. Steglich, J. Aarts, C. D. Bredl, W. Lieke, D. Meschede, W. Franz, and H. Schäfer, Phys. Rev. Lett. **43**, 1892 (1979).
[8] F. Reinert, D. Ehm, S. Schmidt, G. Nicolay, S. Hüfner, J. Kroha, O. Trovarelli, and C. Geibel, Phys. Rev. Lett. **87**, 106401 (2001).
[9] O. Trovarelli, C. Geibel, S. Mederle, C. Langhammer, F. M. Grosche, P. Gegenwart, M. Lang, G. Sparn, and F. Steglich, Phys. Rev. Lett. **85**, 626 (2000); P. Gegenwart, J. Custers, C. Geibel, K. Neumaier, T. Tayama, K. Tenya, O. Trovarelli, and F. Steglich, *ibid.* **89**, 056402 (2002); J. Custers, P. Gegenwart, H. Wilhelm, K. Neumaier, Y. Tokiwa, O. Trovarelli, C. Geibel, F. Steglich, C. Pépin, and P. Coleman, Nature (London) **424**, 524 (2003); J. Sichelschmidt, V. A. Ivanshin, J. Ferstl, C. Geibel, and F. Steglich, Phys. Rev. Lett. **91**, 156401 (2003).
[10] Z. Hossain, C. Geibel, F. Weickert, T. Radu, Y. Tokiwa, H. Jeevan, P. Gegenwart, and F. Steglich, Phys. Rev. B **72**, 094411 (2005).
[11] P. W. Anderson, Phys. Rev. **124**, 41 (1961).
[12] O. Gunnarsson and K. Schönhammer, Phys. Rev. Lett. **50**, 604 (1983); Phys. Rev. B **28**, 4315 (1983).
[13] F. Patthey, J.-M. Imer, W.-D. Schneider, H. Beck, Y. Baer, and B. Delley, Phys. Rev. B **42**, 8864 (1990); L. H. Tjeng, S.-J. Oh, E.-J. Cho, H.-J. Lin, C. T. Chen, G.-H. Gweon, J.-H. Park, J. W. Allen, T. Suzuki, M. S. Makivic, and D. L. Cox, Phys. Rev. Lett. **71**, 1419 (1993); M. Garnier, K. Breuer, D. Purdie, M. Hengsberger, Y. Baer, and B. Delley, *ibid.* **78**, 4127 (1997); T. Okane, S.-I. Fujimori, A. Ino, A. Fujimori, S. K. Dhar, C. Mitra, P. Manfrinetti, A. Palenzona, and O. Sakai, Phys. Rev. B **65**, 125102 (2002).
[14] R. I. R. Blyth, J. J. Joyce, A. J. Arko, P. C. Canfield, A. B. Andrews, Z. Fisk, J. D. Thompson, R. J. Bartlett, P. Riseborough, J. Tang, and J. M. Lawrence, Phys. Rev. B **48**, 9497 (1993).
[15] H. Sato, K. Yoshikawa, K. Hiraoka, M. Arita, K. Fujimoto, K. Kojima, T. Muro, Y. Saitoh, A. Sekiyama, S. Suga, and M. Taniguchi, Phys. Rev. B **69**, 165101 (2004).
[16] A. N. Tahvildar-Zadeh, M. Jarrell, and J. K. Freericks, Phys. Rev. Lett. **80**, 5168 (1998).
[17] M.-W. Xiao, Z.-Z. Li, and Wang Xu, Phys. Rev. B **65**, 235122 (2002).
[18] J. J. Joyce, A. B. Andrews, A. J. Arko, R. J. Bartlett, R. I. R. Blyth, C. G. Olson, P. J. Benning, P. C. Canfield, and D. M. Poirier, Phys. Rev. B **54**, 17515 (1996).
[19] J. J. Joyce, A. J. Arko, A. B. Andrews, and R. I. R. Blyth, Phys. Rev. Lett. **72**, 1774 (1994).
[20] J. M. Lawrence, A. J. Arko, J. J. Joyce, P. C. Canfield, Z. Fisk, J. D. Thompson, and R. J. Bartlett, J. Magn. Magn. Mater. **108**, 215 (1992).
[21] T. Susaki, Y. Takeda, M. Arita, K. Mamiya, A. Fujimori, K. Shimada, H. Namatame, M. Taniguchi, N. Shimizu, F. Iga, and T. Takabatake, Phys. Rev. Lett. **82**, 992 (1999).
[22] J. J. Joyce and A. J. Arko, Phys. Rev. Lett. **78**, 1831 (1997).
[23] T. Susaki, T. Konishi, A. Sekiyama, T. Mizokawa, A. Fujimori, T. Iwasaki, S. Ueda, T. Matsushita, S. Suga, H. Ishii, F. Iga, and M. Kasaya, Phys. Rev. B **56**, 13727 (1997).
[24] T. Susaki, A. Sekiyama, K. Kobayashi, T. Mizokawa, A. Fujimori, M. Tsunekawa, T. Muro, T. Matsushita, S. Suga, H. Ishii, T. Hanyu, A. Kimura, H. Namatame, M. Taniguchi, T. Miyahara, F. Iga, M. Kasaya, and H. Harima, Phys. Rev. Lett. **77**, 4269 (1996).
[25] K. Yoshikawa, H. Sato, M. Arita, Y. Takeda, K. Hiraoka, K. Kojima, K. Tsuji, H. Namatame, and M. Taniguchi, Phys. Rev. B **72**, 165106 (2005).
[26] H. Sato, K. Shimada, M. Arita, K. Hiraoka, K. Kojima, Y. Takeda, K. Yoshikawa, M. Sawada, M. Nakatake, H. Namatame, M. Taniguchi, Y. Takata, E. Ikenaga, S. Shin, K. Kobayashi, K. Tamasaku, Y. Nishino, D. Miwa, M. Yabashi, and T. Ishikawa, Phys. Rev. Lett. **93**, 246404 (2004).
[27] F. Reinert, R. Claessen, G. Nicolay, D. Ehm, S. Hüfner, W. P. Ellis, G.-H. Gweon, J. W. Allen, B. Kindler, and W. Assmus, Phys. Rev. B **63**, 197102 (2001).
[28] J. J. Joyce, A. J. Arko, L. Morales, J. L. Sarrao, and H. Höchst, Phys. Rev. B **63**, 197101 (2001).
[29] D. P. Moore, J. J. Joyce, A. J. Arko, J. L. Sarrao, L. Morales, H. Höchst, and Y. D. Chuang, Phys. Rev. B **62**, 16492 (2000).
[30] F. Reinert, R. Claessen, G. Nicolay, D. Ehm, S. Hüfner, W. P. Ellis, G.-H. Gweon, J. W. Allen, B. Kindler, and W. Assmus, Phys. Rev. B **58**, 12808 (1998).
[31] S. Danzenbächer, Yu. Kucherenko, C. Laubschat, D. V. Vyalikh, Z. Hossain, C. Geibel, X. J. Zhou, W. L. Yang, N. Mannella, Z. Hussain, Z. X. Shen, and S. L. Molodtsov, Phys. Rev. Lett. **96**, 106402 (2006).
[32] D. V. Vyalikh, Yu. Kucherenko, S. Danzenbächer, Yu. S. Dedkov, C. Laubschat, and S. L. Molodtsov, Phys. Rev. Lett. **96**, 026404 (2006).
[33] A. B. Andrews, J. J. Joyce, A. J. Arko, Z. Fisk, and P. S. Riseborough, Phys. Rev. B **53**, 3317 (1996).
[34] H. Kumigashira, S. H. Yang, T. Yokoya, A. Chainani, T. Taka-

hashi, A. Uesawa, T. Suzuki, O. Sakai, and Y. Kaneta, Phys. Rev. B **54**, 9341 (1996).
[35] H. Kumigashira, S. H. Yang, T. Yokoya, A. Chainani, T. Takahashi, A. Uesawa, and T. Suzuki, Phys. Rev. B **55**, R3355 (1997).
[36] A. J. Arko, J. J. Joyce, A. B. Andrews, J. D. Thompson, J. L. Smith, D. Mandrus, M. F. Hundley, A. L. Cornelius, E. Moshopoulou, Z. Fisk, P. C. Canfield, and A. Menovsky, Phys. Rev. B **56**, R7041 (1997).
[37] M. Garnier, D. Purdie, K. Breuer, M. Hengsberger, and Y. Baer, Phys. Rev. B **56**, R11399 (1997).
[38] J. Boysen, P. Segovia, S. L. Molodtsov, W. Schneider, A. Ionov, M. Richter, and C. Laubschat, J. Alloys Compd. **275-277**, 493 (1998).
[39] A. B. Andrews, J. J. Joyce, A. J. Arko, J. D. Thompson, J. Tang, J. M. Lawrence, and J. C. Hemminger, Phys. Rev. B **51**, 3277 (1995).
[40] S. Danzenbächer, Yu. Kucherenko, M. Heber, D. V. Vyalikh, S. L. Molodtsov, V. D. P. Servedio, and C. Laubschat, Phys. Rev. B **72**, 033104 (2005).
[41] H. F. Braun, N. Engel, and E. Parthe, Phys. Rev. B **28**, 1389 (1983).
[42] J. J. Yeh and I. Lindau, At. Data Nucl. Data Tables **32**, 1 (1985).
[43] F. Gerken, J. Phys. F: Met. Phys. **13**, 703 (1983).
[44] W. D. Schneider, C. Laubschat, and B. Reihl, Phys. Rev. B **27**, 6538 (1983).
[45] V. V. Nemoshkalenko, A. E. Krasovskii, V. N. Antonov, Vl. N. Antonov, U. Fleck, H. Wonn, and P. Ziesche, Phys. Status Solidi B **120**, 283 (1983).
[46] O. K. Andersen, Phys. Rev. B **12**, 3060 (1975).
[47] V. I. Anisimov, F. Aryasetiawan, and A. I. Lichtenstein, J. Phys.: Condens. Matter **9**, 767 (1997).
[48] R. Hayn, Yu. Kucherenko, J. J. Hinarejos, S. L. Molodtsov, and C. Laubschat, Phys. Rev. B **64**, 115106 (2001).
[49] P. Rennert, J. Electron Spectrosc. Relat. Phenom. **119**, 1 (2001).
[50] D. A. Varshalovich, A. N. Moskalev, and V. K. Khersonskii, *Quantum Theory of Angular Momentum* (World Scientific, Singapore, 1988).
[51] S. Doniach, Phys. Rev. B **35**, 1814 (1987).